ACS APPLIED MATERIALS & INTERFACES

Research Article

www.acsami.org

Bioorthogonal Layer-by-Layer Encapsulation of Pancreatic Islets via Hyperbranched Polymers

Kerim M. Gattás-Asfura[†] and Cherie L. Stabler*[,†,‡,§,⊥]

[†]Diabetes Research Institute, University of Miami, Miami, Florida 33136 United States

[‡]Department of Biomedical Engineering, University of Miami, Coral Gables, Florida 33146 United States

[§]Department of Surgery, Miller School of Medicine, University of Miami, Miami, Florida 33136 United States

[⊥]Department of Biochemistry and Molecular Biology, Miller School of Medicine, University of Miami, Miami, Florida 33136 United States

Supporting Information

ABSTRACT: Encapsulation of viable tissues via layer-by-layer polymer assembly provides a versatile platform for cell surface engineering, with nanoscale control over the capsule properties. Herein, we report the development of a hyperbranched polymer-based, ultrathin capsule architecture expressing bioorthogonal functionality and tailored physiochemical properties. Random carbodiimide-based condensation of 3,5-dicarboxyphenyl glycineamide on alginate yielded a highly branched polysaccharide with multiple, spatially restricted, and readily functionalizable terminal carboxylate moieties. Poly(ethylene glycol) (PEG) was utilized to link azido end groups to the structured alginate. Together with a phosphine-functionalized poly(amidoamine) dendrimer, nanoscale layer-by-layer coatings, covalently stabilized via Staudinger ligation, were assembled onto solid surfaces and pancreatic islets. The effects of electrostatic and/or bioorthogonal covalent interlayer interactions on the resulting coating efficiency and stability, as well as pancreatic islet viability and function, were studied. These hyperbranched polymers provide a flexible platform for the formation of covalently stabilized, ultrathin coatings on viable cells and tissues. In addition, the hyperbranched nature of the polymers presents a highly functionalized surface capable of bioorthogonal conjugation of additional bioactive or labeling motifs.

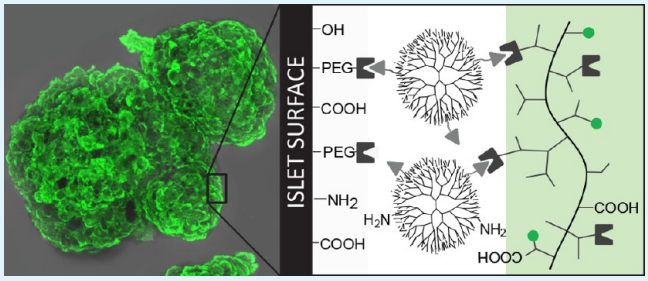

KEYWORDS: *layer-by-layer, Staudinger ligation, dendritic polymer, conformal coating, cell encapsulation*

INTRODUCTION

Pancreatic islet transplantation is a promising treatment for type 1 diabetes mellitus. Current clinical protocols, however, require the use of systemic immunosuppressive drugs to prevent allograft islet rejection, imposing a significant burden on the patient and limiting widespread applicability.[1] Alternatively, islet encapsulation within semipermeable membranes can dampen host immune reactivity to the transplanted tissue by blocking direct alloantigen recognition.[2,3] Further, inflammatory pathways may be dampened via the masking of inflammatory proteins and agents with benign polymers.

Approaches in the encapsulation of pancreatic islets vary from simple PEGylation to more elaborate semipermeable protective membranes.[4] Typically, islets are encapsulated within microscale hydrogel-based beads, on the order of 600−1000 μm;[3,5] however, imposing large barriers between the cell surface and its environment commonly leads to impairment of cellular function and responsiveness, while also substantially increasing the overall volume of the implant.[6,7] Cellular encapsulation via layer-by-layer (LbL) film deposition is a highly desirable technique, wherein the chemical and physical properties of the coating can be precisely tailored at the nanometer scale, resulting in ultrathin, conformal coatings. A variety of intermolecular interactions can be employed to facilitate layer formation, such as electrostatic,[8,9] covalent,[10,11] hydrogen-bonding,[12] and molecular recognition.[13] The most common type of coating strategy, electrostatic complexation, exhibits major drawbacks when applied to encapsulating viable cells, including cytotoxicity of cationic polymers and long-term instability of the resulting coatings. Modulating the net positive charge of cationic polymers, e.g., poly(ethylene glycol) (PEG) polymer grafting, can minimize cell damage,[9] although long-term stability still presents a challenge.

The stability and homogeneity of LbL coatings can be enhanced through the incorporation of interpolymer covalent bonding, which further permits the use of moderately charged or even neutral polymers. While covalent cross-linking within polymeric layers has been achieved through multiple ligation strategies,[10,11,14] the use of bioorthogonal reactions, i.e., orthogonal reactions that can proceed in an aqueous environ-

Received: May 24, 2013
Accepted: September 24, 2013
Published: September 24, 2013

 © 2013 American Chemical Society

ment, under defined environmental conditions (e.g., temperature 25−37 °C, pH 7−7.5, osmolarity ∼300 mOsM), and involve nonnative chemical handles and nontoxic catalysts and/or reaction byproducts[15,16] are highly desirable for viable cell encapsulation. Staudinger ligation, a reaction between an azide and phosphine to form an amide bond, meets these criteria.[17] Not only is the reaction scheme bioorthogonal, but the resulting covalent bond is resistant to hydrolysis, oxidation, and reduction.[18] We have recently demonstrated the applicability of this ligation scheme for enhancing the stability of hydrogels for microscale cellular encapsulation.[19,20]

The use of hyperbranched polymers and dendrimers in the LbL assembly offers a facile platform, with a high degree of end groups for ease in functionalization and efficiency in covalent cross-linking, modulation of chemical property (e.g., biodegradability and stimuli-responsive), and spatially restrictive functional end groups. The latter is important for the efficient LbL assembly of polymers containing hydrophobic functional end groups, such as triphenylphosphine. Hyperbranched polymers have been utilized for a variety of biomedical applications, such as drug-delivery carriers,[21] biosensors,[22,23] transfection,[24] protective coatings,[15] and the self-assembly of multimolecular structures.[25]

Considering that alternate deposition of dendrimer and hyperbranched polymers on surfaces may result in coating materials with tunable properties, this study utilizes these highly branched polymers to assemble an innovative capsule architecture expressing bioorthogonal functionality and tailored physiochemical properties for cellular encapsulation and cell surface engineering. Specifically, we have developed hyperbranched alginate and poly(amidoamine) (PAMAM) dendrimers functionalized with the complementary Staudinger ligation reactive groups, azide and methyl-2-(diphenylphosphino)terephthalate, respectively (Scheme 1). Alginate was selected as the polymeric backbone for hyper-

Scheme 1. Synthetic Steps for the Generation of Hyperbranched Alg-N_3 and MDT/GA PAMAM[a]

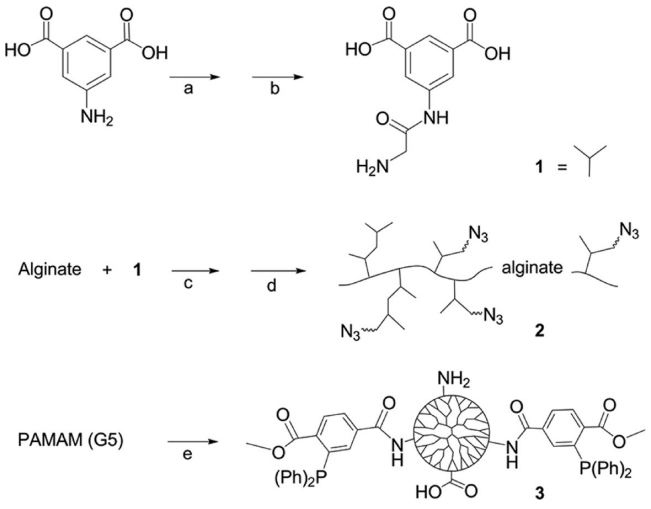

[a]Specifically (1) 3,5-dicarboxyphenyl glycineamide; (2) hyperbranched alginate azide; and (3) PAMAM functionalized with MDT and GA. Key: (a) chloroacetyl chloride and NaOH; (b) NH_3; (c) EDC and NHS; (d) H_2N-PEG-N_3, EDC, and NHS; (e) 2-(diphenylphosphino)terephthalic acid 1-methyl-4-pentafluorophenyl diester, triethylamine, and GA.

grafting because of its known biocompatibility. The effects of polymer functionalization and electrostatic interactions on the efficiency of coating and resulting film stability were evaluated. Subsequently, selected polymers were used to generate ultrathin coatings on viable cell spheroids, specifically pancreatic rat islets (Scheme 2), whereby the resulting cytotoxicity and cellular function were evaluated. The implications of this novel bioorthogonal, covalent, LbL platform for cell surface engineering, as well as postfunctionalization of terminal end groups for chemoselective conjugation of additional bioactive motifs, are discussed.

MATERIAL AND METHODS

Materials. Sodium alginate (PRONOVA UP VLVG; M_w 29 kDa, G/M ratio ≥ 1.5) was purchased from NovaMatrix. Fluorescein-5-thiosemicarbazide was purchased from Marker Gene Technologies. A Thermo Scientific SnakeSkin regenerated cellulose membrane of 22 mm and 10 kDa molecular weight (MW) cutoff was used for dialysis. (11-Bromoundecyl)trichlorosilane was purchased from Gelest. Silicon wafers (single side polished, no dopant, 2 in. diameter × 0.5 mm thickness), TSKgel GMPWxl (1−8000 kDa MW range) column, poly(amidoamine) (PAMAM; 5% w/v in methanol, ethylenediamine core, generation 5, MW 28826 g/mol, 5.4 nm diameter, 128 primary amino end groups), 4-pentafluorophenyl ester of 1-methyl-2-(diphenylphosphino)terephthalic acid (MDT-pfp), organic solvents, and other high-purity reagents were purchased from Sigma-Aldrich. Culture buffers and CMRL media were purchased from Cellgro and Gibco, respectively. Cell viability stains and picogreen DNA determination assays were purchased from Invitrogen. An insulin quantification ELISA assay was purchased from Mercodia.

Polymer Characterization. A PerkinElmer Spectrum 100 spectrometer was utilized to obtain attenuated total reflectance Fourier transform infrared (ATR-FT-IR) spectra for all samples. Spectra were an average of four scans at 4 cm^{-1} resolution. The spectrometer was equipped with a KBr beam splitter, an electronically and temperature stabilized fast-recovery deuterated triglycine sulfate detector, and a 1 bounce universal ATR sampling accessory. ^1H NMR spectra for all samples were obtained using a Bruker 400 MHz NMR with an autotuning multinuclear probe, housed at the Chemistry Department of the University of Miami. Dynamic light scattering (DLS) measurements were obtained on a Wyatt Technology DynaPro Titan DLS instrument. A total of 10 reads were performed for each sample, with at least three independent assessments for each tested polymer and polymer mixtures. Dextran of varying MWs (from 10 to 500 kDa) were used to correlate the *z*-average radius to its respective MW. For *z*-average radii above 10 nm, a logarithmic fit was used, based on the collected dextran calibration curve (R^2 = 0.994). For *z*-average radii between 1 and 10 nm, a linear fit was used, again based on the collected dextran calibration curve within that range (R^2 = 0.969). Matrix-assisted laser desorption/ionization time-of-flight mass spectrometry (MALDI-TOF-MS; Bruker Bi-Flex IV) measurements with α-cyano-4-hydroxycinnamic acid as the matrix were used for the MW assessment of N_3-PEG-NHS (Chemistry Department, University of Miami). MALDI was attempted for hyperbranched alginate, but was unsuccessful. A Hitachi LaChrom Elite high-performance liquid chromatograph, a TSKgel GMPWxl (1−8000 kDa MW range) column, and a flow rate of 0.6 mL/min were used for size-exclusion chromatography (SEC). Hyperbranched alginate azide (0.2 mg/mL), labeled with FITC, and FITC−dextran calibrations of 10, 70, or 500 kDa (0.01 mg/mL) were tested. A fluorescence detector recorded emission at 520 nm upon excitation at wavelength 480 nm. FITC was used to enhance measurement sensitivity. Phosphate-buffered saline (PBS; 1x, pH 7.4, 135 mM NaCl) was used as the elution and solvent buffer. To fully and rapidly solubilize Hyp-Alg-N_3, the pH of the solution was adjusted to 12 with 5 M NaOH and mixed well, followed by deliberate pH neutralization to 7.2 via 5 M HCl.

Synthesis of 3,5-Dicarboxyphenylglycineamide. The synthesis protocol for 3,5-dicarboxyphenylglycineamide was adapted

Scheme 2. Schematic of Ultrathin Coating Assembly[a]

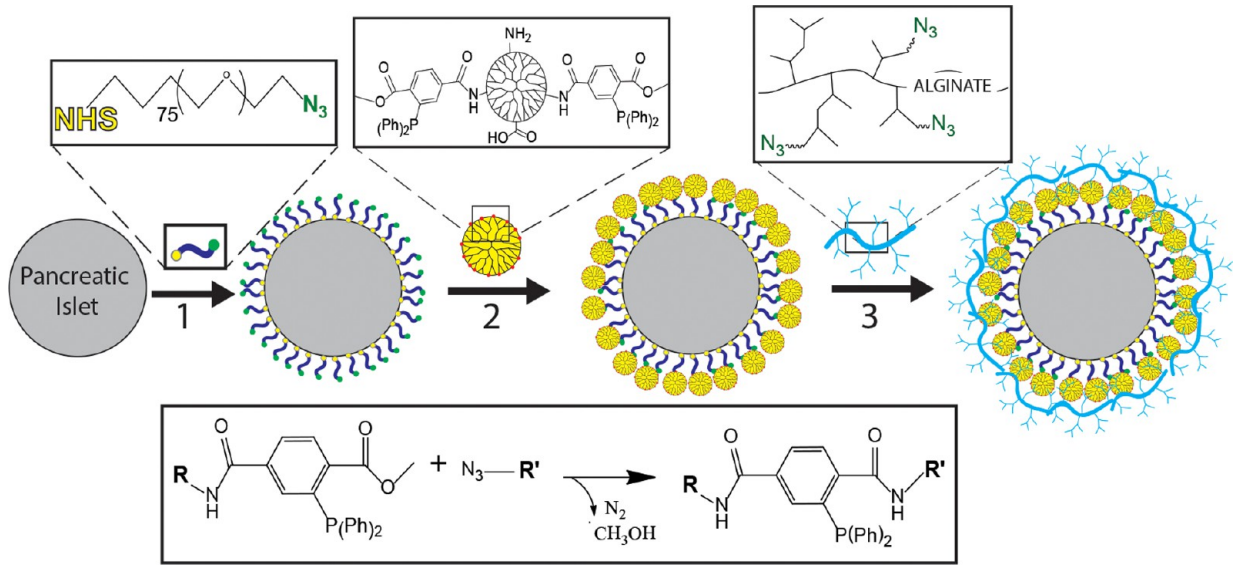

[a]For electrostatic assembly, MDT-functionalized PAMAM (2) is deposited directly onto the islet surface via electrostatic interactions. For covalent assembly, N_3-PEG-NHS is first covalently bound to free amines on the islet surface (1), followed by covalent linkage of MDT-functionalized PAMAM (2). Subsequently, hyperbranched alginate azide is covalently linked to the exposed MDT-functionalized PAMAM coating (3). Interlayer covalent bonds are formed between complementary azide and MDT groups via Staudinger ligation (inset reaction scheme). Additional layers can be built via the stepwise incubation of MDT-functionalized PAMAM (2) and hyperbranched alginate azide (3), until the desired number of layers is achieved.

from the literature.[26] First, 2 mL of chloroacetyl chloride was added at a rate of 500 μL every 10 min to a stirring solution containing 5 g of 5-aminoisophthalic acid, dissolved in 60 mL of 4 M NaOH while cooling the flask over an ice−water bath. After 20 min, the pH of the solution was adjusted to 1.5 with 10 M HCl. A precipitate formed and was collected by filtration, rinsed with cold water, and dried under reduced pressure. The yield was 5.9 g of a light brown solid with selected characteristic ATR-FT-IR bands at 3336, 3222, 2901, 2636, 1715, 1689, 1631, 1562, 790, 767, 750, and 700 cm^{-1}.

Next, 5 g of the above product (3,5-dicarboxyphenylchloroacetamide) was reacted overnight with 70 mL of 29.5% aqueous ammonia. Ammonia was removed under reduced pressure. The resulting solution was cooled in an ice−water bath, and the pH was adjusted to 1 with 10 M HCl. The resulting precipitate was collected via filtration, rinsed with cold water, and dried under reduced pressure. The yield was 2.1 g of a light brown solid. Kaiser's test was positive. Selected characteristic ATR-FT-IR bands were found at 3088, 2611, 1917, 1688, 1618, 1550, 1386, 1211, 899, and 759 cm^{-1}. ^{1}H NMR (D_2O with 0.05% TSP and NaOH): δ 3.89 (2H), 8.04 (2H), 8.12 (1H).

Synthesis of Hyperbranched Alginate. A mixture of 200 mg of alginate, 16 mg of *N*-hydroxysuccinimide (NHS), 240 mg of 2-(*N*-morpholino)ethanesulfonic acid (MES), and 20 mL of purified water was stirred until fully dissolved. 1-Ethyl-3-[3-(dimethylamino)propyl]-carbodiimide (EDC; 800 mg) was added in small incremental portions. Subsequently, 200 mg of 3,5-dicarboxyphenylglycineamide, dissolved in 3.8 mL of a 0.42 M NaOH solution, was added at a rate of 267 μL/min under agitation. After 25 min, 240 μL of 5 M NaOH was added at a rate of 2.67 μL/min. The product was precipitated with 40 mL of acetone, collected by filtration, rinsed twice with 4 mL of acetone, dissolved in 4 mL of 50 mM NaCl, precipitated with 8 mL of acetone, rinsed twice with 33% (v/v) water in acetone, rinsed twice with 8 mL of acetone, and dried under reduced pressure. The yield was 350 mg of a white crystalline-like solid with selected characteristic ATR-FT-IR bands at 3271, 3087, 2934, 1694, 1607, 1565, 1396, 1361, 1088, and 1024 cm^{-1}.

Azido Functionalization of Hyperbranched Alginate. The amounts of 50 mg of hyperbranched alginate, 5 mg of NHS, 30 mg of MES, 50 mg of H_2N-PEG-N_3 (M_w of 372 g/mol, synthesized as previously reported[19]), and either 0 or 2 mg of fluorescein-5-thiosemicarbazide were dissolved in 5 mL of purified water. In small portions, 125 mg of EDC was added with stirring. After 20 min, 30 μL of 5 M NaOH was added at a rate of 1 μL/min. The product was precipitated with 20 mL of acetone, collected by centrifugation (2643*g* for 2 min), dissolved twice in 3 mL of 50 mM NaCl, precipitated with 15 mL of acetone, rinsed twice with 15 mL of acetone, and dried under reduced pressure. The resulting dried precipitate was dissolved in 4 mL of deionized water and purified via dialysis against 500 mL of water (replaced every 20 min for 2 h). For the first hour, 10 μL of 5 M NaOH and 200 μL of 1 M NaCl were introduced to the solution within the dialysis bag every 20 min. The pure solution was filter-sterilized (0.2-μm-pore-size filter) and freeze-dried. The yield was 54 mg of a white or orange solid. Kaiser's test was negative. Selected ATR-FT-IR bands: 3278, 2877, 2110, 1645, 1600, 1540 cm^{-1}. ^{1}H NMR (D_2O with 0.05% TSP): δ 2.24, 2.84, 3.28−3.82, 7.52−8.48. MW: ^{1}H NMR = 76 kDa average MW, based on end-group analysis and the average MW of the base alginate of 29 kDa (for details on calculation of the degree of end-group functionalization, see the Results and Discussion section); SEC = 65−850 kDa, based on the dextran calibration curve, and DLS = 70−250 kDa, based on the *z*-average hydrodynamic radius and dextran calibration curve. Of note, a broad MW distribution was expected for the hyperbranched alginate because of the nature of hypergrafting and alginate monodispersity.[27,28] In addition, SEC and DLS methods are affected by polymer aggregation in solution, which may contribute to the wider MW range detected by these techniques.[29−31]

MDT Functionalization of PAMAM. A solution of 14, 28, or 37 mg of MDT-pfp in 500 μL of anhydrous dichloromethane (DCM) was dropwise injected into 1 mL of 5% w/v PAMAM in methanol under an argon atmosphere and stirred for 30 min. For selected PAMAM-MDT, where glutaric anhydride (GA) was added, 25 μL of triethylamine in 500 μL of DCM was first dropwise injected, followed by the slow injection of 0−10 mg of GA in 500 μL of DCM. After stirring for an additional 30 min, 20 μL of glacial acetic acid was added. The product was precipitated with 10 mL of diethyl ether and collected by centrifugation (200*g* for 1 min). The resulting precipitate was dissolved or suspended in 1 mL of 50% v/v DCM in methanol with vortex under an argon atmosphere, precipitated with 10 mL of diethyl ether, collected by centrifugation, and dried under reduced

pressure. The product was dissolved in 2 mL of purified water containing 20 μL of glacial acetic acid; otherwise, the pH was increased with NaOH until dissolved. The solution was purified by dialysis for 2 h against 500 mL of purified water (replaced every 20 min) under constant argon bubbling. During the first hour, 100 μL of 1 M NaCl was added every 20 min. The resulting solution was filter-sterilized and freeze-dried. Successful functionalization and chemical moieties were confirmed by ^{1}H NMR and ATR-FT-IR spectroscopy. The yield was 52−57 mg. Selected ATR-FT-IR bands: 1717, 1637, 1539, 746, 697 cm^{-1}. ^{1}H NMR (D_2O with 0.05% TSP): δ 1.83, 2.07−3.66, 6.5−8.2. Additional characteristics, including MW, are listed in Table 1.

Table 1. Properties of Selected PAMAM Derivatives with Varying MDT and GA Functionalization

PAMAM (ID)	MDT (%)	GA (%)	net charge	MW (g/mol)
30/0	29	0	+91	41670
15/0	14	0	+110	35026
15/20	14	23	+51	38412
15/30	14	35	+21	40178
15/40	14	44	−3	41503
15/50	14	58	−38	43564

Synthesis of N_3-PEG-NHS. First, 34 mg of GA in 500 μL of DCM was injected at a rate of 8 μL/min into 1 g of H_2N-PEG-NH_2 (M_w of 3513 g/mol, synthesized as previously reported[19]) dissolved in 5 mL of DCM with rapid stirring and reacted for 2 h under an argon atmosphere. DCM was removed under reduced pressure. The product was dissolved in 7 mL of purified water and passed through a 20 mL column of QAE-Sephadex beads using water as the solvent. The collected eluted samples containing PEG were combined and freeze-dried. PEG was detected by a precipitation test upon mixing of the same volumes of samples with 1% poly(acrylic acid) in a 1 N HCl solution. The above procedure was repeated, using SP-Sephadex beads instead. The resulting solid was dissolved in 5 mL of anhydrous DCM, filtered through a polypropylene filter (0.45 μm pore size), and dried under reduced pressure. The yield was 460 mg of a white solid powder. Kaiser's test was positive. Selected characteristic ATR-FT-IR bands: 2883, 1652, 1552, 1099 cm^{-1}. ^{1}H NMR ($CDCl_3$ with 0.03% TMS): δ 1.92−2.03 (m, 2H), 2.28−2.45 (dt, 4H, J = 6.06−7.07 Hz), 3.65 (s, 354H), 6.46 (s, 1H), 7.91 (s, 2H).

Second, 200 mg of the product from step 1 (H_2N-PEG-COOH) was reacted with 49 mg of N_3-PEG-NHS (M_w of 914 g/mol, synthesized as previously reported[32]) and 31 μL of triethylamine in 700 μL of anhydrous *N*,*N*-dimethylformamide (DMF) for 25 min under an argon atmosphere. The product was precipitated with 7 mL of cold (ice−water bath) diethyl ether, collected by centrifugation (2643*g* for 5 min at 0 °C), dissolved in 7 mL of 200 proof ethanol at 37 °C, passed through a silica gel pad (5 × 15 mm in a Pasteur pipet), precipitated by cooling in an ice−water bath with frequent vortex, collected by centrifugation, rinsed with 7 mL of cold diethyl ether, and dried under reduced pressure. The yield was 0.17 g of a white solid. Kaiser's test was negative. Selected characteristic ATR-FT-IR bands: 2884, 2105, 1732, 1660, 1544, 1102 cm^{-1}.

Finally, 140 mg of the product from step 2 (N_3-PEG-COOH) was reacted with 11 mg of NHS and 30 μL of *N*,*N*′-diisopropylcarbodiimide in 500 μL of anhydrous DMF for 2 h under an argon atmosphere. The product was precipitated with 5 mL of cold diethyl ether, collected by centrifugation (2643*g* for 5 min at 0 °C), dissolved in 5 mL of 200 proof ethanol at 37 °C, precipitated by cooling in an ice−water bath with frequent vortex, collected by centrifugation, rinsed with 5 mL of cold diethyl ether, and dried under reduced pressure. The yield was 120 mg of a white solid powder. Selected characteristic ATR-FT-IR bands: 2884, 2105, 1812, 1782, 1739, 1668, 1543, 1207, 1100 cm^{-1}. ^{1}H NMR ($CDCl_3$ with 0.03% TMS): δ 1.92−2.42 (11H), 2.63−2.98 (5H), 3.13−3.87 (498H). M_w by MALDI was 4023 g/mol.

Azido Functionalization of Silicon Wafers. A silicon wafer was cut to approximately 11 × 13 mm. It was treated with 2 mL of 0.1 M NaOH for 3 min at 80 °C, rinsed three times with 2 mL of pure water, once with 2 mL of 0.1 M HCl, three times with 2 mL of water, and three times with 2 mL of ethanol, and blow-dried with argon. The wafer was then treated with 6 μL of (11-bromoundecyl)trichlorosilane in 2 mL of toluene for 30 min at 80 °C under an argon atmosphere and frequent swirling. The silicon wafer was rinsed three times with 2 mL of toluene, three times with 2 mL of 5% (v/v) water in DMF, and three times with 2 mL of ethanol, blow-dried with argon, and cured at 110 °C for 10 min under an argon atmosphere. Finally, the silicon wafer was treated with 10 mg of NaN_3 in 2 mL of anhydrous DMF under an argon atmosphere for 1 h at 80 °C and frequent swirling. The silicon wafer was rinsed three times with 2 mL of DMF, six times with 2 mL of pure water, three times with 2 mL of 50% (v/v) water in ethanol, and three times with 2 mL of ethanol, blow-dried with argon, and stored under argon at 4 °C in the dark.

Coating and Characterization of Azido-Functionalized Silicon Wafers. For each layer deposited, a silicon wafer was placed in a Petri dish with a water reservoir and covered to prevent dehydration. The azido-functionalized surface was covered with the specific polymeric solution at 3 mg/mL in PBS (1x, pH 7.4) and incubated for 10 min at 37 °C. The solution was mixed two or three times during incubation via a pipet. A large test tube and pipet were utilized to rinse the wafer three times with PBS and deionized water and blow-dry with argon. The film thickness on silicon wafer surfaces was measured with a J. A. Woollam Co. α-SETM spectroscopic ellipsometer at a 70° angle in standard mode. Data were fitted to the "Si with transparent film" model. Samples for elemental composition of the surface films on silicon wafers were submitted to the NanoScience Technology Center of the University of Central Florida for X-ray photoelectron spectroscopy (XPS; Physical Electronics 5400 ESCA).

Coating of Pancreatic Islets. Lewis rat islets were isolated as described previously.[33] Islets were coated 48 h postisolation. Islets were transferred into a 15 mL polypropylene centrifuge tube and pelleted by centrifugation (682 rpm for 14 s). For the electrostatic assembly of layers, islets were suspended in a 3 mg/mL polymeric solution (in supplemented CMRL1066 culture media) for 30 s at room temperature. The CMRL medium was supplemented with 8.7% (v/v) fetal bovine serum (HyClone from Thermo Scientific), 330 mg/L of L-glutamine, 96 U/mL of penicillin, 96 mg/L of streptomycin, and 22 mL/L of a 1 M HEPES buffer.

For the covalent assembly of each layer, islets were first reacted with N_3-PEG-NHS at 20 mg/mL in PBS (1x, supplemented with 0.3 mg/mL of D-glucose, pH 7.8) for 20 min at room temperature. To deposit additional PAMAM or hyperbranched alginate layers, islets were incubated in a 3 mg/mL polymeric solution (in supplemented CMRL1066 culture media) for 10 min at 37 °C.

The coating uniformity and stability was assessed 24 and 120 h following the LbL assembly via detection of fluorescently labeled hyperbranched alginate. Images were collected using a Leica SP5 spectral confocal inverted microscope. Multislice images (4−8 μm thickness; 50−110 slices per image; 1024 × 1024; 20× objective) were collected and compiled using a 3D projection function. Islets were assessed via MTT metabolic activity, live/dead imaging, and glucose stimulated insulin secretion, as previously described.[34] For MTT, triplicates of 300 IEQ were evaluated. MTT results were normalized to control values and represented as a fold change from control absorbance. For insulin evaluation, triplicates of 100 IEQ were assessed. A rat ELISA kit (Mercordia) and a Molecular Devices SpectraMax M5 microplate/cuvette reader were utilized to quantify insulin levels. Coated islets were also assessed via transmission electron microscopy (TEM) 24 h after coating. Islets were pelleted and immersed in 2% glutaraldehyde. The fixed islets were then embedded in an Epon/Araldite resin, sectioned, mounted on grids, and stained with 4% uranyl acetate (in 100% methanol) for TEM imaging. TEM images were obtained using a Jeol Jem-1400 transmission electron microscope operating at 80 kV.

For bioorthogonal labeling of the ultrathin coating, islets were coated with nonfluorescently labeled polymers. Following the assembly of layers, the control and coated islets were incubated with 3 mg/mL of FITC-PEG_{5000}-MDT or FITC-PEG_{5000}-CH_3 (control) for

30 min. Confocal imaging of the resulting coatings was performed as described above.

Statistical Analysis. Data are expressed as the mean ± standard deviation, with $n \geq 3$ for each experimental group. A minimum of three independent experiments were made for each assay, with graphs summarizing the results from a representative experiment. For islet viability and insulin secretion experiments, comparisons between groups were made only using the same islet preparation, to minimize variations due to islet isolation procedures. Statistical analysis was performed on all samples using one-way ANOVA and a Tukey multiple comparison test to evaluate significant differences between groups with $P < 0.05$.

RESULTS AND DISCUSSION

Characterization of Dendritic Polymers. Synthetic steps and illustrations of hyperbranched polymers are summarized in

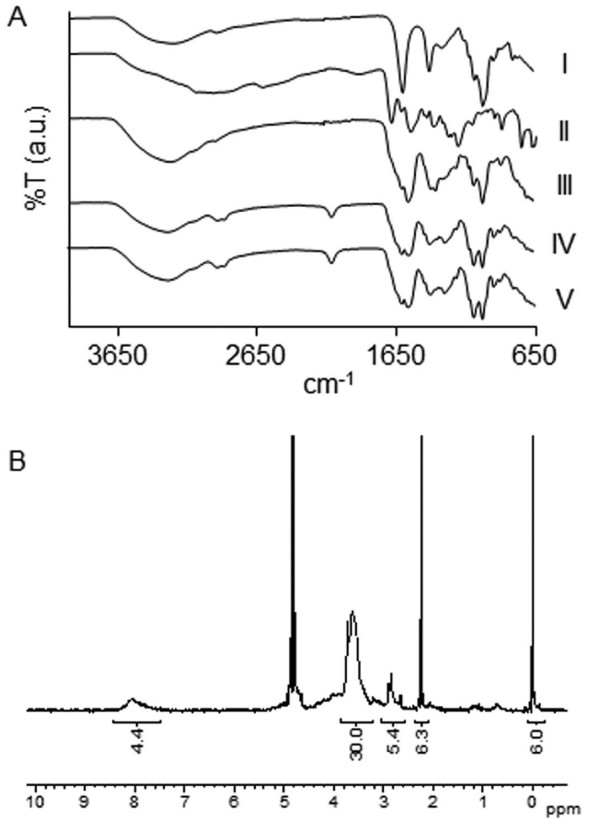

Figure 1. Characterization of hyperbranched alginate. (A) ATR-FT-IR spectra of (I) alginate, (II) 3,5-dicarboxyphenylglycineamide, (III) hyperbranched alginate, (IV) hyperbranched alginate azide, and (V) fluorescent hyperbranched alginate azide. (B) ^{1}H NMR of hyperbranched alginate azide.

Scheme 1. A convenient one-pot carbodiimide-based coupling protocol was utilized to hypergraft branched polymeric chains of 3,5-dicarboxyphenylglycineamide onto the alginate backbone. Subsequently, hyperbranched alginate was functionalized with linear, heterobifunctional PEG (M_w 350 g/mol), expressing a primary amino and an azido end group. The resulting condensation reaction formed stable amide bonds. ATR-FT-IR spectroscopy exhibited characteristic vibrational bands of hyperbranched alginate azide (Alg-N_3), including the alginate O−H stretch (3278 cm^{-1}), alginate CO_2^- asymmetric stretch (1600 cm^{-1}), amide C═O stretch (1645 cm^{-1}), amide N−H bending (1540 cm^{-1}), PEG C−H symmetric stretch (2877 cm^{-1}), and azide asymmetric stretch (2110 cm^{-1})

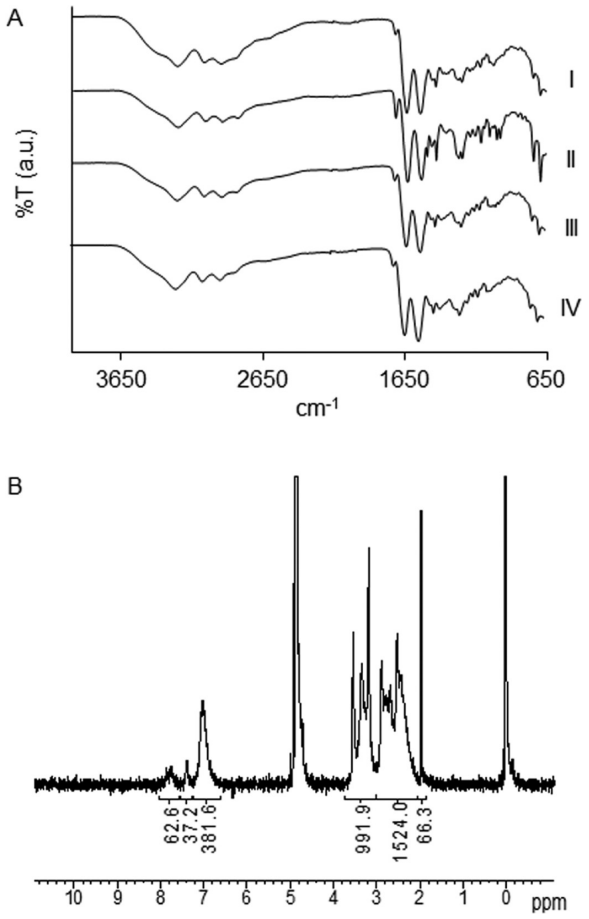

Figure 2. Characterization of PAMAM dendrimers. (A) ATR-FT-IR spectra of (I) PAMAM 15/0, (II) PAMAM 30/0, (III) PAMAM 15/20, and (IV) PAMAM 15/40. (B) ^{1}H NMR of PAMAM 30/0.

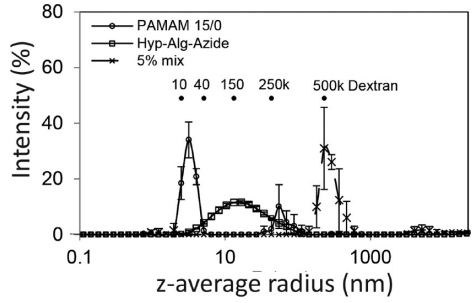

Figure 3. Assessment of the particle size via DLS for PAMAM 15/0 (3 mg/mL), Hyp-Alg-azide (3 mg/mL), and a mixture of PAMAM 15/0 (3 mg/mL) with Hyp-Alg-azide (0.15 mg/mL or 5%). Error = SD; N = 3.

(Figure 1A). The degree of functionalization was derived from ^{1}H NMR spectroscopy and peak integration (Figure 1B). A calibration curve of PEG (δ 3.28−3.82) at different concentrations against the constant TSP standard was also used to determine the degree of PEG on the sample. The integration ratio between PEG and aromatic ring protons (δ 7.52−8.48) was used to quantify the amount of 3,5-dicarboxyphenylglycineamide. Subtracting the derived weights of PEG and 3,5-dicarboxyphenylglycineamide from that of the sample in solution provided the amount of alginate. Data indicated that 1 mol of alginate had 106 mol of 3,5-dicarboxyphenylglycineamide and 70 mol of H_2N-PEG-N_3,

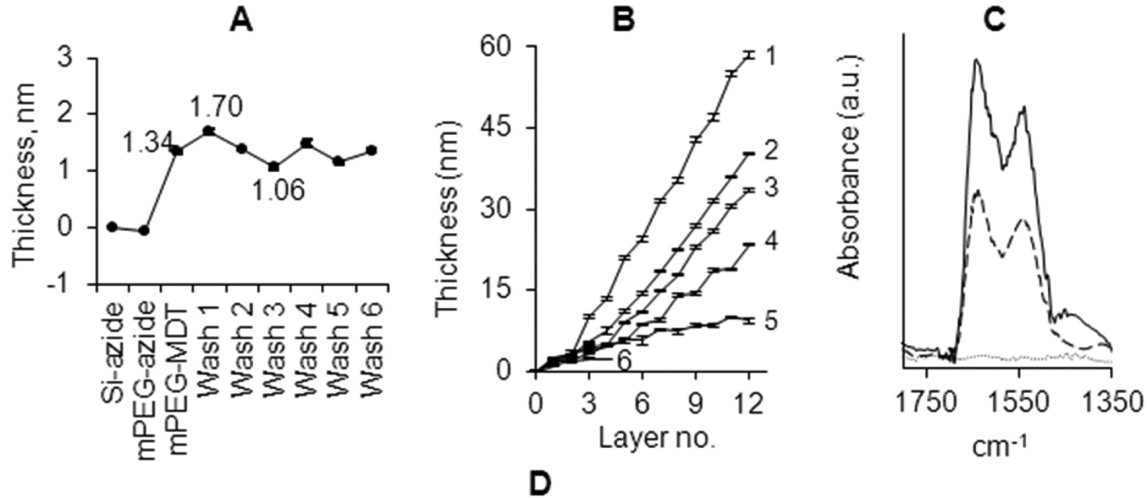

D

No. Layers	PAMAM	Alginate	Thickness (nm)	%C (1s)	%N (1s)	%O (1s)	%P (2p)	%Si (2p)
4	40/0	Hyp. Alg-N_3	16.4	63.21	11.61	24.14	0.90	0.14
12	0/0	Hyp. Alg	17.4	61.93	14.55	23.17	0.00	0.34
0	---	---	---	24.54	1.34	35.67	---	38.44

Figure 4. LbL assembly of functionalized hyperbranched alginate and PAMAM polymers on planar substrates. (A) Selectivity and stability of an azide-functionalized silicon wafer illustrated via incubation of the silicone azide surface with mPEG-N_3 (control), followed by incubation with mPEG-MDT (bioorthogonal conjugation). The wafer was subsequently washed with PBS (washes 1−3), followed by 4 M NaCl (washes 4−6). (B) Ellipsometry film thickness measurements on planar azide-functionalized silicon surfaces after deposition of 12 alternating polymeric layers of either (1) PAMAM 30/0 with hyperbranched Alg-N_3, (2) PAMAM 15/0 with hyperbranched Alg-N_3, or (3) PAMAM 15/40 with hyperbranched Alg-N_3. The controls consisted of (4) PAMAM 0/0 with hyperbranched alginate, (5) PAMAM 15/40 with hyperbranched alginate, and (6) PAMAM 15/40 with Alg-N_3 (not hyperbranched). Error = standard deviation. (C) ATR-FT-IR spectra of the deposited films (2, solid line), (3, dashed line), and control (uncoated, gray line). (D) Elemental composition of the surfaces of silicon wafers by XPS.

exhibiting a functionalization increase of greater than 350% over our previous nonbranched, alginate functionalization method.[19]

For fabrication of a MDT-functionalized PAMAM dendrimer, 15, 30, or 40% functionalization of primary amino end groups on PAMAM with MDT was evaluated. All resulting PAMAMs were soluble in PBS; however, solutions of 40% functionalized PAMAM turned cloudy upon warming to 37 °C and were thus excluded from further study. The resulting PAMAM was highly cationic (Table 1). A decreased positive or net neutral polyelectrolyte composition may be more desirable for cellular encapsulation, given that reduction of the polymer cationic strength tends to increase the biocompatibility.[35] As such, to manipulate the net surface charge of the dendrimer, a subset of the remaining primary amino groups was subsequently reacted with GA. Functionalization of 30% MDT-functionalized PAMAM with 15−30% GA resulted in aggregation at 37 °C. Thus, MDT functionalization was decreased to 15% to permit soluble PAMAMs with GA functionalization. ATR-FT-IR spectra of PAMAM MDT/GA dendrimers revealed characteristic bands of the MDT group (1719, 746, and 697 cm^{-1}), as well as amide bonding (1637 and 1539 cm^{-1}) (Figure 2A). The degree of functionalization was determined via the NMR peak integration ratio between aromatic (δ 6.5−8.2) or GA (δ 1.83) against PAMAM (δ 2.07−3.66) protons (Figure 2B). Characterization data of selected MDT- and GA-functionalized PAMAM dendrimers are summarized in Table 1. Of note, the surface net charge listed for the specific dendrimer assumes that every primary amino or carboxylate group is charged; thus, the true net charge depends on the pH of the solution. Through manipulation of the MDT and GA functionalization, variation in the degree of covalent linkage points, as well as the overall cationic charge of the polymer, can be modulated. This degree of control permits evaluation of the effects of electrostatic and/or covalent interactions on the film formation, thickness, and stability.

Polymers were further assessed via DLS, which provides evaluation of the *z*-average hydrodynamic radius (r) of the polymers. As shown in Figure 3, PAMAM 15/0 peaked at r = 3.2 nm, while hyperbranched Alg-N_3 exhibited a broad distribution centered at r = 15.0 nm. Random grafting and branching of the polysaccharide backbone may be a contributing factor for the lack of *z*-average hydrodynamic radius homogeneity for the hyperbranched alginate. The heterogeneity of the polymer size was further supported by SEC (see Figure S-1 in the Supporting Information, SI). Of interest, the addition of a small amount (0.15 mg/mL) of the hyperbranched polymer to the functionalized PAMAM solution reproducibly resulted in instant shifting of the *z*-average hydrodynamic radius to r = 292 nm (Figure 3).

Coating of the Silicon Wafer. The ability of these complementary polymers to form stable, covalently linked coatings in a LbL manner was first evaluated using idealized silicon planar substrates functionalized with azide groups. Azido functionalization of silicon wafers was confirmed via selective binding of mPEG-MDT (but not mPEG-N_3) on the silicon surface (Figure 4A). The resulting polymer coating was found to be stable upon repeated rinsing with PBS and 4 M NaCl (Figure 4A). Varying combinations of MDT/GA-functionalized PAMAM and hyperbranched Alg-N_3 polymers were screened for their capacity for LbL assembly, specifically (1) PAMAM 30/0 with hyperbranched Alg-N_3, (2) PAMAM 15/0 with

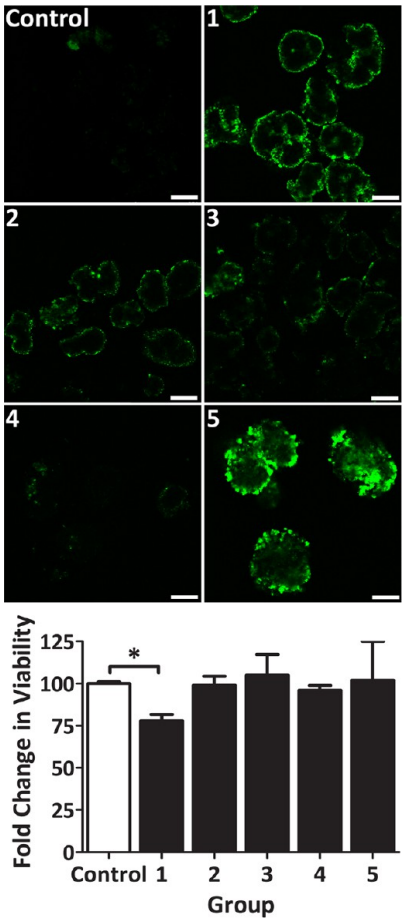

Figure 5. Coating uniformity and cell viability of primary rat pancreatic islets following three-layer encapsulation via PAMAM and alginate. Single-plane, confocal fluorescent images of rat islet cross sections 24 h postencapsulation with three-layer coatings. Islet viability, via MTT metabolic assay, normalized to the control (graph). Groups: uncoated (control); three-layer coating using either PAMAM 15/0 (1), 15/20 (2), 15/30 (3), or 15/40 (4), interlayered with fluorescently labeled hyperbranched Alg-N_3 (5); NHS-PEG-N_3, followed by three-layer coating using PAMAM 15/40 interlayered with fluorescently labeled hyperbranched Alg-N_3. Error = standard deviation. Scale bar = 200 μm. (*) $P < 0.05$.

hyperbranched Alg-N_3, and (3) PAMAM 15/40 with hyperbranched Alg-N_3. Efficient and complete LbL polymer deposition was achieved for all experimental groups (Figure 4B), with the film thickness linearly increasing ($R^2 \geq 0.99$) after deposition of the third layer. Control groups consisted of (4) PAMAM 0/0 with hyperbranched alginate, (5) PAMAM 15/40 with hyperbranched alginate, and (6) PAMAM 15/40 with Alg-N_3 (not hyperbranched). For highly cationic dendrimers (e.g., PAMAM 0/0, 15/0, and 30/0), covalent interactions were not required for LbL assembly (e.g., Figure 4B, no. 4); however, interpolymer covalent bonding led to thicker individual polymeric layers. For example, increasing MDT functionalization from 0 to 15% to 30% (i.e., PAMAM 0/0 to 15/0 to 30/0) resulted in increased film thickness (Figure 4B, no. 4 to no. 2 to no. 1). A comparison of the films formed using cationic (PAMAM 15/0) and neutral (PAMAM 15/40) dendrimers of identical MDT functionalization (Figure 4B, nos. 2 and 3) found that increased cationic charge resulted in a moderate increase in the overall film thickness; highlighting the benefits, but not the requirement, of electrostatic attraction to efficient film deposition. For neutral dendrimers (PAMAM 15/40), covalent linkages were critical for LbL assembly, as illustrated by comparing films formed using hyperbranched alginate with or without azide functionalization (Figure 4B, no. 3 vs no. 5); emphasizing the importance of covalent linkages in film deposition when electrostatic interactions were absent. Negatively charged PAMAM dendrimers (e.g., PAMAM 15/50) did not exhibit LbL deposition with hyperbranched Alg-N_3, likely due to electrostatic repulsion between the negatively charged PAMAM and alginate polymers (see Figure S-2 in the SI).

Covalently linked films were found to be highly stable over time in both PBS buffer and 4 M NaCl solutions at 37 °C (<1% decrease in the film thickness) compared to films generated solely via electrostatic interactions (8.5 and 20% loss in film thickness following PBS and NaCl washes, respectively). Overall, while film assembly was successful through either covalent or electrostatic interactions, the combination of covalent and electrostatic interactions resulted in the largest overall film thickness and greatest stability.

Of note, LbL film deposition was not achieved when a nonhyperbranched Alg-N_3 was used with PAMAM 15/40 (Figure 4B, no. 6). Hence, the hyperbranches are responsible, at least in part, for the observed layer formation. It has been reported in the literature that LbL film assemblies of poly(allylamine hydrochloride) (PAH) incorporating poly(styrenesulfonate), which contains similar negative (sulfonate) groups on benzene rings, exhibit strong colloidal stability because of their charge density and pK_a.[36] Thus, the resulting strong polyelectrolyte nature of the hyperbranched alginate could be the contributing factor; however, other nonspecific interactions such as $\pi-\pi$ stacking, π–cation interaction, and hydrogen bonding could contribute to the observed assembly and stability of the films.

ATR-FT-IR spectra of coated silicon wafers confirmed successful film deposition by the appearance of two IR bands centered at 1647 and 1549 cm^{-1}, principally corresponding to the amide I and II bonds, respectively, on the assembled films (Figure 4C). ATR-FT-IR spectra revealed higher IR absorbance for the polymer combination resulting in both electrostatic and covalent interactions (**2**), in agreement with ellipsometric measurements. XPS characterization of selected uncoated versus coated films further confirmed ellipsometric and ATR-FT-IR results, whereby multilayer films containing MDT-functionalized PAMAM had detectable phosphorus levels (Figure 4D).

Coating of Primary Pancreatic Islets. The ability of complementary PAMAM and alginate polymers to form nanothin, covalently stabilized, polymeric films on cell clusters was evaluated using primary pancreatic rat islets (Scheme 2). An initial evaluation of the islet coating and resulting cytotoxicity was performed via deposition of three polymer layers: PAMAM dendrimer, hyperbranched Alg-N_3 (labeled with fluorescein for imaging), and PAMAM dendrimer. In this manner, the first layer assembled onto the islet via electrostatic or, possibly hydrogen bonding, only. For this preliminary three-layer assessment, PAMAM derivatives 15/0, 15/20, 15/30, and 15/40 were screened. Ultrathin, conformal coatings were observed on islet spheroids (Figure 5; nos. 1–4); however, a trend of decreasing fluorescent intensity and coating uniformity with decreasing PAMAM cationic charge was observed, with minimal detection of fluorescence for the net neutral PAMAM 15/40. These results indicate that the final film assembly using

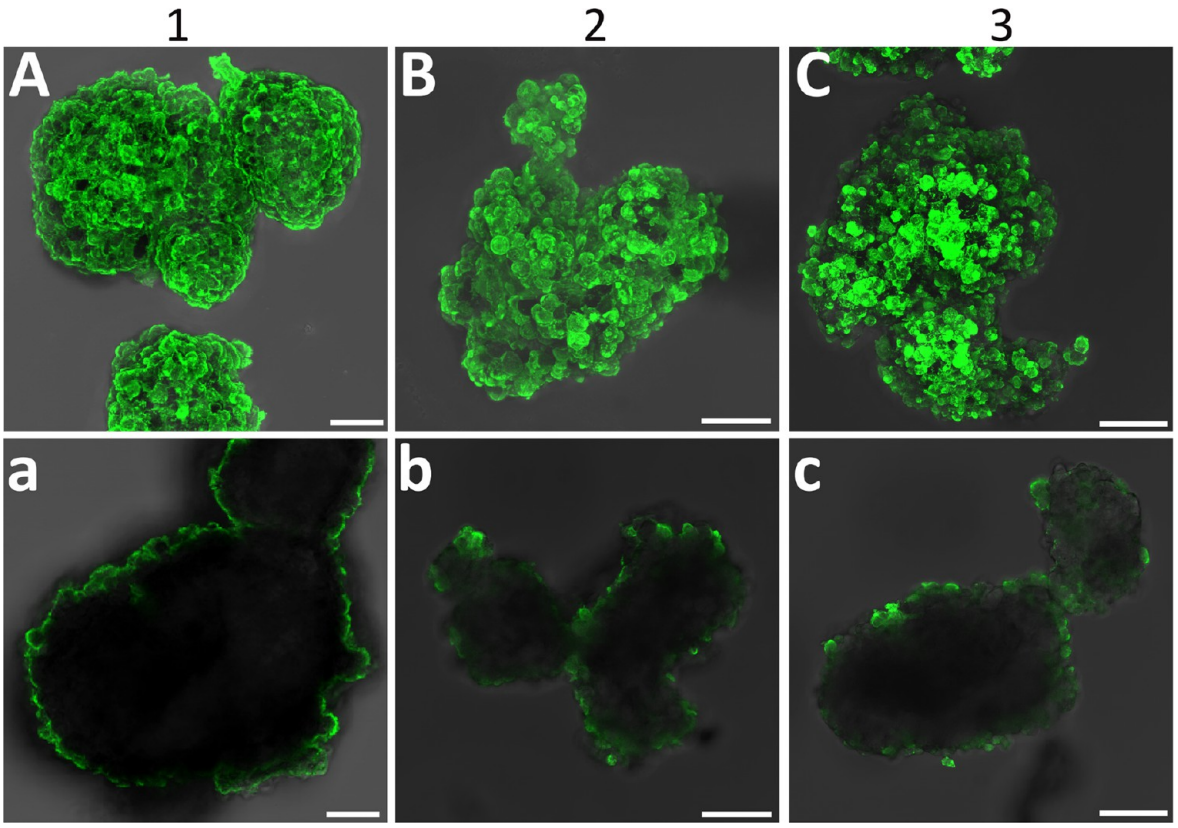

Figure 6. Six-layer encapsulation of primary rat pancreatic islets via LbL assembly of alginate and PAMAM. Evaluation of capsule formation via fluorescein-labeled alginate and confocal *z*-stack projection (A−C) or single-plane (a−c) imaging of rat pancreatic islets 24 h after coating. Groups: (1) electrostatic assembly via three bilayers of PAMAM 15/0 and fluorescently labeled hyperbranched Alg-N_3; (2) primary layer of NHS-PEG-N_3, followed by three bilayers of PAMAM 15/20 and fluorescently labeled hyperbranched Alg-N_3; (3) primary layer of NHS-PEG-N_3, followed by three bilayers of PAMAM 15/40 and fluorescently labeled hyperbranched Alg-N_3. Scale bar = 50 μm.

this approach was dependent on electrostatic interactions at the primary layer. The LbL uniformity using a neutral PAMAM polymer was enhanced via the addition of a primary PEG-N_3 layer onto the islet surface through incubation of islets with NHS-PEG-N_3. PEG coating was achieved via NHS ester conjugation with primary amino groups on the islet's surface. Incubation of PEG-N_3-coated islets with PAMAM 15/40 resulted in a significant increase in the overall LbL assembly (Figure 5, no. 4 vs no. 5). These results illustrate the ability to form LbL coatings on islets using neutral PAMAM dendrimers, once the islet surface was terminated in azido groups.

Assessment of the cellular viability following the three-layer coating procedure via MTT metabolic assay (Figure 5) revealed that highly cationic PAMAM dendrimers, e.g., PAMAM 15/0, were cytotoxic, resulting in decreased overall metabolic activity. The cytotoxicity was concentration- and time-dependent (e.g., metabolic activity decreased from 97 to 27% when the PAMAM 30/0 concentration and incubation time were increased from 0.1 mg/mL/1 min to 3.5 mg/mL/30 min). This trend in the cytotoxicity was expected, as the toxicity of highly cationic polymers, such as poly(L-lysine) (PLL) and PAH, for numerous cell types has long been documented.[13,35,37] Charge neutralization via GA by 20% or higher (e.g., PAMAM 15/20, 15/30, and 15/40) decreased the cytotoxicity, consistent with published reports on the neutralization of cationic polymers, such as PEG grafting of PLL.[37] After 3 days of culture, resulting three-layer coatings revealed instability, with coating fragmentation was observed.

Following three-layer screening of polymer combinations, evaluation of the most promising dendrimers, i.e., PAMAM 15/0, 15/20, and 15/40, was performed via the LbL assembly of six total layers. PAMAM 15/0 was layered via electrostatic assembly and directly applied to the islet surface. For PAMAM 15/20 or 15/40, PAMAM was layered onto the cell spheroid following islet PEGylation via NHS-PEG-N_3. For all coatings, fluorescently labeled, hyperbranched Alg-N_3 was utilized as the alternating layer. Following the deposition of six layers of PAMAM and hyperbranched Alg-N_3, nanothin coatings on the islet surface were visualized via confocal microscopy (Figure 6). Strong coverage was observed for coatings containing PAMAM 15/0 or 15/20 dendrimers. A trend of decreased coating coverage was observed as GA functionalization on the PAMAM dendrimer increased. Single-plane images highlight the localization of the coatings to the periphery of the cell spheroid (Figure 6, bottom panel). The presence of ultrathin PAMAM/alginate coatings was further confirmed via TEM. As illustrated in Figure 7, the polymeric coatings were relegated to the islet periphery. The coating thickness, per TEM analysis, ranged from 70 to 100 nm. The consistency of the coating was further verified to be high for coating schemes utilizing PAMAM 15/0 and 15/20, while the coating scheme employing PAMAM 15/40 was found to be irregular.

Confocal images collected 5 days after coating indicated highly stable capsules when PAMAM 15/0 and 15/20 were used, while a moderate decrease in the coating uniformity was detected for PAMAM 15/40 coatings (see Figure S-3 in the SI).

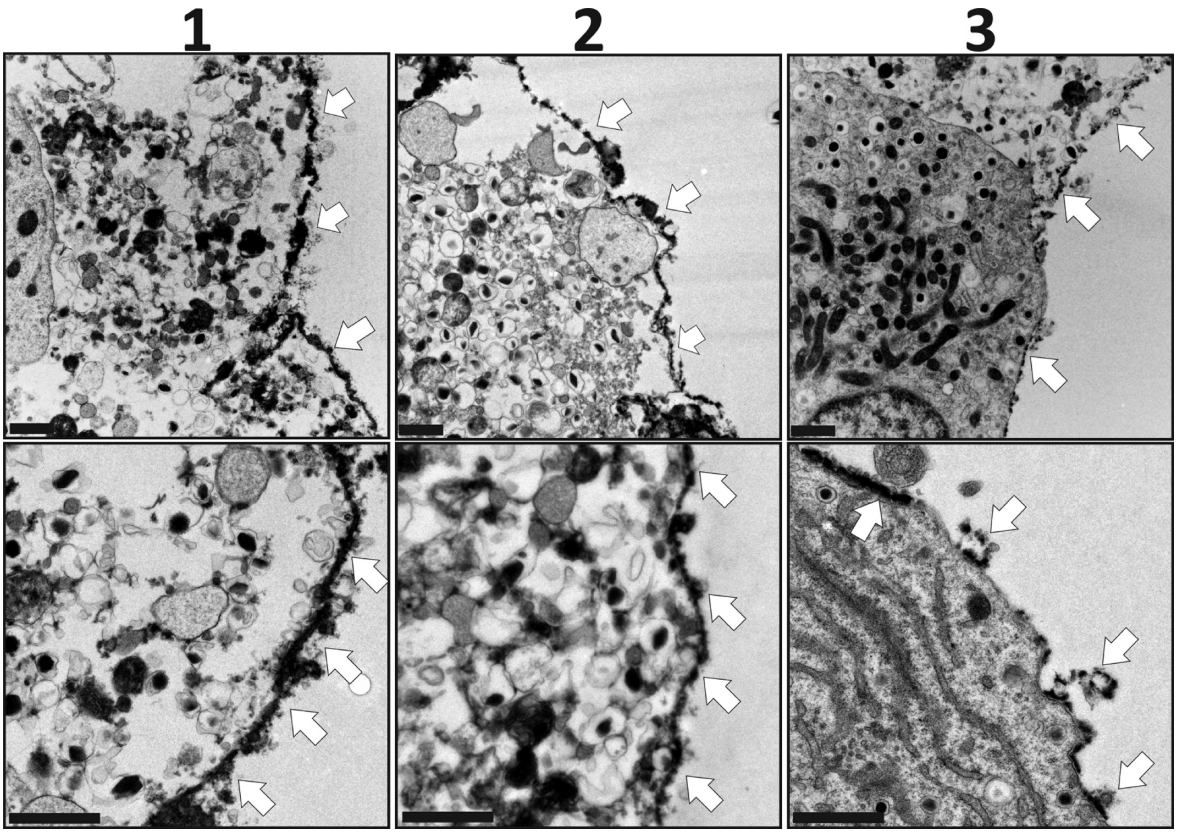

Figure 7. TEM images of primary rat pancreatic islets coated with six layers via LbL assembly of alginate and PAMAM. Groups: (1) electrostatic assembly via three bilayers of PAMAM 15/0 and hyperbranched Alg-N_3; (2) primary layer of NHS-PEG-N_3, followed by three bilayers of PAMAM 15/20 and hyperbranched Alg-N_3; (3) primary layer of NHS-PEG-N_3, followed by three bilayers of PAMAM 15/40 and fluorescently labeled hyperbranched Alg-N_3. Scale bar = 1 μm.

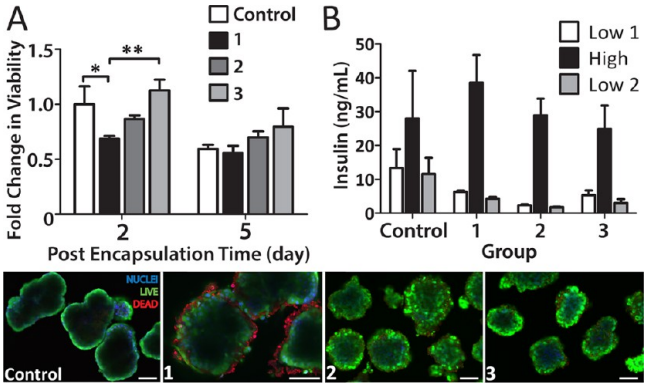

Figure 8. Assessment of the islet viability and function after six-layer coating via MTT metabolic assay (A), glucose-stimulated insulin release (B), and live/dead confocal microscopy imaging (bottom panel; blue, nuclei; live, green; dead, red). Groups: (1) electrostatic assembly via three bilayers of PAMAM 15/0 and fluorescently labeled hyperbranched Alg-N_3; (2) primary layer of NHS-PEG-N_3, followed by three bilayers of PAMAM 15/20 and fluorescently labeled hyperbranched Alg-N_3; (3) primary layer of NHS-PEG-N_3, followed by three bilayers of PAMAM 15/40 and fluorescently labeled hyperbranched Alg-N_3. Note: nonspecific binding of the nuclei staining (ethidium homodimer-1, red fluorescence) was observed for part 1. (*) $P < 0.05$. (**) $P < 0.01$. Scale bar = 50 μm.

The results illustrate the enhanced stability of the resulting covalently stabilized LbL coatings, even for dynamic, viable tissue surfaces, when six polymeric layers were utilized.

The inhomogeneity of the coatings built on a primary NHS-PEG-N_3 layer may be attributed to incomplete saturation of the primary PEG coating on the islet surface. Published reports found that a single treatment with activated ester molecules such as NHS-PEG may not result in complete cell coverage.[38] Thus, future efforts will focus on improving the homogeneity of this PEG base layer via multiple incubations or doping of the islet surface with amine-rich proteins, while preserving islet viability.

Characterization of the islet viability and function following encapsulation with PAMAM and alginate polymers was conducted via live/dead imaging, MTT, and glucose-stimulated insulin secretion. Metabolic assessment of islets 48 h postencapsulation via MTT revealed a significant decrease in the viability for coated islets containing PAMAM 15/0 compared to the controls (Figure 8A). On the contrary, capsules containing PAMAM 15/20 or neutral PAMAM 15/40 resulted in no significant decrease in the overall cell viability compared to the control islets. Tracking the islet viability 5 days postencapsulation found no detectable difference in the viability from the controls because the viability of the control islet significantly decreased from day 2 to day 5 ($P < 0.001$). This decrease in the viability for the control islets was expected, given the trend of decreased viability for islets following long culture times.[39] Of interest, no significant decline in the islet viability from day 2 to day 5 was observed for coated islets, regardless of the polymer combination used.

The islet function and ability of insulin to diffuse out of the coating was evaluated via glucose-stimulated insulin release,

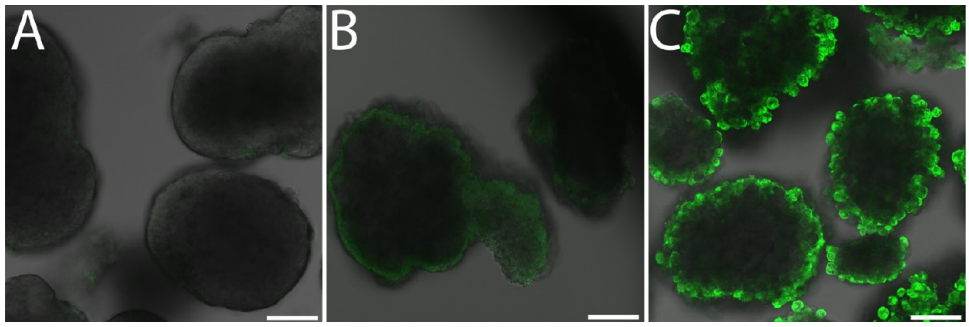

Figure 9. Bioorthogonal tethering of FITC-PEG-MDT to islets following LbL encapsulation. Confocal planar slice image of uncoated control islets incubated in FITC-PEG_{5000}-MDT (A); islet coated with six layers of PAMAM 15/20 and hyperbranched alginate-N_3, followed by incubation with FITC-PEG_{5000}-CH_3 (B); islet coated with six layers of PAMAM 15/20 and hyperbranched alginate-N_3, followed by incubation with FITC-PEG_{5000}-MDT (C). Scale bar = 50 μm.

whereby islets were exposed to 1 h intervals of low, high, and low glucose challenges. All groups exhibited comparable function and responsive insulin secretion when challenged with high glucose (Figure 8B). Live/dead imaging of the coated islets support metabolic activity results, with moderate peripheral cell death observed for islets treated with PAMAM 15/0 (Figure 8, bottom panel). Of note, binding of the red dead cell stain (ethidium homodimer-1) to the highly cationic PAMAM 15/0 was detected, complicating imaging analysis. While this probe was designed to not fluoresce prior to interaction with DNA, coincubation of this probe with functionalized dendritic polymers exhibited red fluorescence (see Figure S-4 in the SI). Counterstaining of cells with hoechst nuclei stain permitted delineation between nonspecific binding and nuclei binding of dead cells.

With establishment of the benign nature of the LbL scheme using PAMAM and hyperbranched alginate polymers, future studies will seek to evaluate the capacity of these coatings to mask incendiary cell markers, as well as impart immunoprotective effects. These studies include extensive evaluation of the coating permselectivity, detailed characterization of the coating uniformity, assessment of the coating's capacity to mask inflammatory proteins and antigens, and in vivo testing using allograft and xenograft transplant models.

Bioorthogonal Labeling of the Ultrathin Coating. While encapsulation with biocompatible polymers is highly desirable for masking the cell surface, engineering the surface to express bioactive motifs could provide additional benefits via modulating the local implant environment to assist engraftment, vascularization, decrease inflammation, and/or direct immune responses. Through the use of highly branched and rigid polymers, the resulting coating surface can express a high degree of either phosphine or azide groups, whereby additional agents of interest, such as labels, particles, or proteins, can be easily tethered, in a bioorthogonal manner, via Staudinger ligation chemistry. We have demonstrated this ability, and its subsequent specificity, using fluorescently labeled PEGs expressing a complementary Staudinger ligation group (Figure 9). Thus, these coatings represent a versatile platform for further surface functionalization via highly chemoselective ligation, which can be desirable for cell and tissue engineering applications.

CONCLUSIONS

We report the development of functionalized hyperbranched alginate and dendritic polymers that provide a facile platform for the generation of tailored, covalently stabilized, ultrathin coatings on inert and viable surfaces. Hyperbranched structures were found to facilitate efficient, uniform, and stable film deposition. Due to the cytocompatibility of the bioorthogonal ligation strategy, coated pancreatic islets exhibited unimpaired viability and function when the dendrimer cationic strength was mitigated. With the high stability of the resulting coatings and film deposition efficiency, these conformal coating systems may find potential applications in the immunoprotection of islets for the treatment of diabetes. Furthermore, the flexibility of this platform to bioorthogonally tether supplemental agents to the surface provides an additional tool to modulate the implant microenvironment.

ASSOCIATED CONTENT

Supporting Information

SEC results, change in the film thickness upon deposition of alternate layers of PAMAM 15/50 and hyperbranched Alg-N_3, encapsulation of primary rat pancreatic islets via six layers via the LbL assembly of alginate and PAMAM, and fluorescence intensity of ethidium homodimer-1 probe following mixing with dendritic materials in solution. This material is available free of charge via the Internet at http://pubs.acs.org.

AUTHOR INFORMATION

Corresponding Author

*E-mail: cstabler@med.miami.edu.

Notes

The authors declare the following competing financial interest(s): K.G.A. and C.L.S. have pending patent applications regarding the technology presented in this manuscript.

ACKNOWLEDGMENTS

This work was supported by the National Institutes of Health through the type 1 Diabetes Pathfinder Award Program (1DP2 DK08309601) and the Diabetes Research Institute Foundation. We thank the DRI Preclinical and Translational Models Core for providing the rodent islets used for this study and the DRI Analytical Imaging Core for use of their facilities. We thank the University of Central Florida Advanced Materials Processing and Analysis Center, in particular Kirk Scammon, for XPS measurements and analysis. We thank the University of Miami EM Core, particularly Peggy Bates, Vania Almeida, and Yelena Pressman, for their highly efficient TEM processing and imaging. We especially thank Dr. Camillo Ricordi, Director of

the Diabetes Research Institute, for his continual guidance, support, and consult.

REFERENCES

(1) Barton, F. B.; Rickels, M. R.; Alejandro, R.; Hering, B. J.; Wease, S.; Naziruddin, B.; Oberholzer, J.; Odorico, J. S.; Garfinkel, M. R.; Levy, M.; Pattou, F.; Berney, T.; Secchi, A.; Messinger, S.; Senior, P. A.; Maffi, P.; Posselt, A.; Stock, P. G.; Kaufman, D. B.; Luo, X.; Kandeel, F.; Cagliero, E.; Turgeon, N. A.; Witkowski, P.; Naji, A.; O'Connell, P. J.; Greenbaum, C.; Kudva, Y. C.; Brayman, K. L.; Aull, M. J.; Larsen, C.; Kay, T. W.; Fernandez, L. A.; Vantyghem, M. C.; Bellin, M.; Shapiro, A. M. *Diabetes Care* **2012**, *35*, 1436−1445.
(2) Giraldo, J. A.; Weaver, J. D.; Stabler, C. L. *J. Diabetes Sci. Technol.* **2010**, *4*, 1238−1247.
(3) Teramura, Y.; Iwata, H. *Adv. Drug Delivery Rev.* **2010**, *62*, 827−840.
(4) Scharp, D. W.; Marchetti, P. *Adv. Drug Delivery Rev.* **2013**, DOI: 10.1016/j.addr.2013.07.018.
(5) Lim, F.; Sun, A. *Science* **1980**, *210*, 908−910.
(6) Trivedi, N.; Keegan, M.; Steil, G. M.; Hollister-Lock, J.; Hasenkamp, W. M.; Colton, C. K.; Bonner-Weir, S.; Weir, G. C. *Transplantation* **2001**, *71*, 203−211.
(7) van Schilfgaarde, R.; de Vos, P. *J. Mol. Med.* **1999**, *77*, 199−205.
(8) Zhi, Z. L.; Kerby, A.; King, A. J.; Jones, P. M.; Pickup, J. C. *Diabetologia* **2012**, *55*, 1081−1090.
(9) Wilson, J. T.; Cui, W.; Kozlovskaya, V.; Kharlampieva, E.; Pan, D.; Qu, Z.; Krishnamurthy, V. R.; Mets, J.; Kumar, V.; Wen, J.; Song, Y.; Tsukruk, V. V.; Chaikof, E. L. *J. Am. Chem. Soc.* **2011**, *133*, 7054−7064.
(10) El Haitami, A. E.; Thomann, J.-S. b.; Jierry, L. c.; Parat, A.; Voegel, J.-C.; Schaaf, P.; Senger, B.; Boulmedais, F.; Frisch, B. t. *Langmuir* **2010**, *26*, 12351−12357.
(11) Buck, M. E.; Lynn, D. M. *Adv. Eng. Mater.* **2011**, *13*, B343−B352.
(12) Kozlovskaya, V.; Zavgorodnya, O.; Chen, Y.; Ellis, K.; Tse, H. M.; Cui, X.; Thompson, J. A.; Kharlampieva, E. *Adv. Funct. Mater.* **2012**, *22*, 3389−3398.
(13) Wilson, J. T.; Cui, W.; Chaikof, E. L. *Nano Lett.* **2008**, *8*, 1940−1948.
(14) Such, G. K.; Quinn, J. F.; Quinn, A.; Tjipto, E.; Caruso, F. *J. Am. Chem. Soc.* **2006**, *128*, 9318−9319.
(15) Paez, J. I.; Brunetti, V.; Strumia, M. C.; Becherer, T.; Solomun, T.; Miguel, J.; Hermanns, C. F.; Calderon, M.; Haag, R. *J. Mater. Chem.* **2012**, *22*, 19488−19497.
(16) Best, M. D. *Biochemistry (Moscow)* **2009**, *48*, 6571−6584.
(17) Saxon, E.; Bertozzi, C. R. *Science* **2000**, *287*, 2007−2010.
(18) Saxon, E.; Armstrong, J.; Bertozzi, C. *Org. Lett.* **2000**, *2*, 2141−2143.
(19) Gattás-Asfura, K. M.; Stabler, C. L. *Biomacromolecules* **2009**, *10*, 3122−3129.
(20) Hall, K. K.; Gattás-Asfura, K. M.; Stabler, C. L. *Acta Biomater.* **2011**, *7*, 614−624.
(21) Kaminskas, L. M.; McLeod, V. M.; Porter, C. J. H.; Boyd, B. J. *Mol. Pharm.* **2012**, *9*, 355−373.
(22) Qu, Y.; Sun, Q.; Xiao, F.; Shi, G.; Jin, L. *Bioelectrochemistry* **2010**, *77*, 139−144.
(23) Vieira, N. C. S.; Figueiredo, A.; de Queiroz, A. A. A.; Zucolotto, V.; Guimarães, F. E. G. *Sensors* **2011**, *11*, 9442−9449.
(24) Jin, G.-w.; Koo, H.; Nam, K.; Kim, H.; Lee, S.; Park, J.-S.; Lee, Y. *Polymer* **2011**, *52*, 339−346.
(25) Zhou, Y.; Huang, W.; Liu, J.; Zhu, X.; Yan, D. *Adv. Mater.* **2010**, *22*, 4567−4590.
(26) Vinogradov, S. A. *Org. Lett.* **2005**, *7*, 1761−1764.
(27) Gao, C.; Yan, D. *Prog. Polym. Sci.* **2004**, *29*, 183−275.
(28) Schull, C.; Frey, H. *ACS Macro Lett.* **2012**, *1*, 461−464.
(29) Ahrer, K.; Buchacher, A.; Iberer, G.; Josic, D.; Jungbauer, A. *J. Chromatogr. A* **2003**, *1009*, 89−96.
(30) Nobbmann, U.; Connah, M.; Fish, B.; Varley, P.; Gee, C.; Mulot, S.; Chen, J.; Zhou, L.; Lu, Y.; Shen, F.; Yi, J.; Harding, S. E. *Biotechnol. Genet. Eng. Rev.* **2007**, *24*, 117−28.
(31) Dollinger, G.; Cunico, B.; Kunitani, M.; Johnson, D. L.; Jones, R. *J. Chromatogr. A* **1992**, *592*, 215−228.
(32) Gattás-Asfura, K. M.; Fraker, C. A.; Stabler, C. *J. Biomed. Mater. Res. A* **2011**, *99*, 47−57.
(33) Pileggi, A.; Molano, R. D.; Ricordi, C.; Zahr, E.; Collins, J.; Valdes, R.; Inverardi, L. *Transplantation* **2006**, *81*, 1318−24.
(34) Pedraza, E.; Coronel, M. M.; Fraker, C. A.; Ricordi, C.; Stabler, C. L. *Proc. Natl. Acad. Sci. U. S. A.* **2012**, *109*, 4245−50.
(35) Fischer, D.; Li, Y.; Ahlemeyer, B.; Krieglstein, J.; Kissel, T. *Biomaterials* **2003**, *24*, 1121−1131.
(36) Mak, W. C.; Cheung, K. Y.; Trau, D. *Chem. Mater.* **2008**, *20*, 5475−5484.
(37) Wilson, J. T.; Krishnamurthy, V. R.; Cui, W.; Qu, Z.; Chaikof, E. L. *J. Am. Chem. Soc.* **2009**, *131*, 18228−9.
(38) Lee, D. Y.; Yang, K.; Lee, S.; Chae, S. Y.; Kim, K. W.; Lee, M. K.; Han, D. J.; Byun, Y. *J. Biomed. Mater. Res.* **2002**, *62*, 372−7.
(39) Kin, T.; Senior, P.; O'Gorman, D.; Richer, B.; Salam, A.; Shapiro, A. M. J. *Transplant Int.* **2008**, *21*, 1029−1035.